Supporting Information

Tailoring single-cycle near field in a tunnel junction with carrier-envelope phase-controlled terahertz electric fields

Katsumasa Yoshioka[1], Ikufumi Katayama[1*], Yusuke Arashida[1], Atsuhiko Ban[1],

Yoichi Kawada[2], Kuniaki Konishi[3] Hironori Takahashi[2], and Jun Takeda[1*]

[1]Department of Physics, Graduate School of Engineering, Yokohama National University,

Yokohama 240-8501, Japan

[2]Central Research Laboratory, Hamamatsu Photonics K.K., 5000 Hirakuchi, Hamakita,

Hamamatsu City, Shizuoka 434-8601, Japan

[3]Institute for Photon Science and Technology, Graduate School of Science,

The University of Tokyo, Tokyo 113-0033, Japan

*E-mail: jun@ynu.ac.jp; katayama@ynu.ac.jp.

I. Experimental setup for the THz-STM

Figure S1 shows our experimental setup. We employed a Ti:sapphire regenerative amplifier with a repetition rate, pulse duration, and a center wavelength of 1 kHz, 130 fs and 800 nm, respectively, as the light source. Single-cycle THz electric field transients were generated using a $LiNbO_3$ prism in a tilted-pulse-front configuration [1]. The generated THz pulses were collimated by a gold-coated off-axis parabolic mirror (PM1), and then introduced into a Mach-Zehnder interferometer characterized by a dual-phase double-pulse scheme. The THz pulse was further split into two beams, using an anti-reflection coated silicon beam splitter (Si BS1), which were then used as CEP-controlled and delay-controlled THz pulses. For the CEP-controlled pulses, we used a CEP shifter (applicable to broadband THz pulses) consisting of a quarter-wave plate (THz QWP), a half-wave plate (THz HWP) and a wire grid polarizer (WG1) [2]. The field strength of the THz pulses was tuned using a pair of wire grid polarizers (WG2 and WG4). For the delay-controlled THz pulses, the field strength was tuned using a couple of wire grid polarizers (WG3 and WG4) after passing through a delay stage (DS). The CEP-controlled and delay-controlled pulses were subsequently combined using an anti-reflection coated silicon beam splitter (Si BS2). We used silicon

wafers with different thicknesses (Si BS1 and Si BS2) for adequate reduction of the field strengths associated with the multi-reflection pulses (<20% of the main pulse). The waveform-controlled double THz pulses were then guided into one of two paths by either removing or inserting a removable gold-coated mirror; one path was used for characterizing the THz pulses via electro-optic sampling (EOS) and the other was used for delivering the pulses to a tunnel junction of the STM. For the EOS, we confirmed that identical waveforms occurred for 2-mm-thick ZnTe (110), 1-mm-thick ZnTe (110) and 0.4 mm-thick GaP (110) crystals. The THz pulse energy was calculated by integrating the THz intensity both temporally and spatially [3]. To accurately characterize the THz waveform at the junction, the same off-axis parabolic mirrors (PM2 and PM3; focal length: 4 inches, diameter: 2 inches) were used to focus the THz pulses. The resulting beam diameter at both the STM junction and the EO crystal was 1.2 mm.

The THz tunnel current was recorded by a real-time digital oscilloscope (Tektronics DPO71254C) via the STM circuits. THz pulses were chopped at 500 Hz and the feedback loop was switched on and off with 20 Hz. The CEP-dependent tunnel current
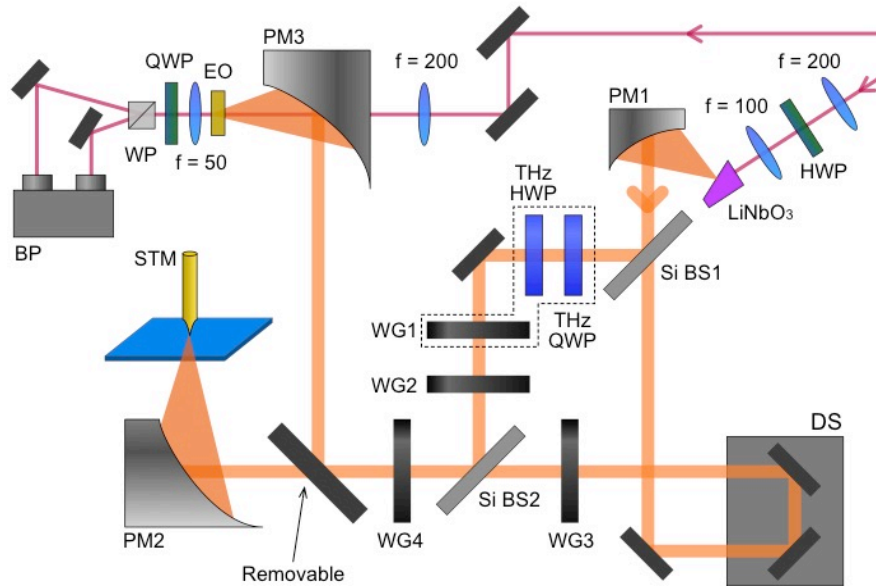

Figure S1 | Experimental setup for THz-STM. Si BS: silicon beam splitter, DS: delay stage, QWP: quarter-wave plate, HWP: half-wave plate, PM: parabolic mirror, WG: wire grid polarizer, EO: electro-optic crystal, WP: Wollaston prism, BP: balanced photodiode. A component of the CEP shifter is enclosed by the dotted line.

(Fig. 1d) was measured by rotating the THz HWP by 180°, which corresponds to a CEP shift of 2π. The data was measured within 4 seconds and the feedback loop remained off during the measurement.

II. Near-field calculation

The values of the effective work function and gap width (3.8 eV and 1.0 nm, respectively) used in the calculations of the tunnel current were obtained from a previous study [4]. Both parameter values were determined by THz-field-induced current data (THz I-V) and current-distance data with a direct current electric field (dc I-Z; see Fig. S2 for the dc I-Z results).

The CEP of near fields in the junction is strongly dependent on the shape of the nanotip (Fig. 3). Therefore, we assume that the CEP shift results from the configurational resonance of a nanotip, as discussed in previous scanning near-field optical microscopy [5,6] and THz streaking spectroscopy investigations of a nanotip [7]. In those studies, the THz near field in the junction was phenomenologically simulated using a generic antenna-model [5–7], where an equivalent RLC circuit was assigned to the nanotip. The relationship between the THz near field at the tip apex $E_{near}(t)$ and the current $I_{THz}(t)$ in an antenna is given as follows:

$$E_{near}(t) \propto \int_{-\infty}^{t} I_{THz}(t')dt',$$

Similarly, the induced current $I_{THz}(\omega)$ in the frequency domain is expressed as:

$$I_{THz}(\omega) \propto \frac{E_{far}(\omega)}{(R + j\omega L - j/(\omega C))},$$

where $E_{far}(\omega)$, R, L and C are the incident THz far field, radiation resistance, inductance and capacitance, respectively. The resonance frequency is determined from $f_0 = 1/(2\pi\sqrt{LC})$. The THz near field in the junction can be retrieved by adjusting the three reactive parameters, thereby yielding the experimental results shown in Fig. 3a. The simulation parameters used for Tip 1, Tip 3 and Tip 5 are summarized in Table S1. An inductive part L is somewhat difficult to understand its origin compared to R and C. However, the results obtained correspond closely to the experimental data, as evidenced by reasonable parameter values, which are similar to those used for THz streaking spectroscopy at a nanotip [7]. We used different effective work functions between the

sample and the nanotip to reproduce the asymmetry of the observed CEP-resolved tunnel currents. Effective work functions of 3.66 eV, 3.73 eV and 3.74 eV were used for Tip 1, Tip 3 and Tip 5, respectively, while an effective work function of 3.80 eV was used for the HOPG sample.
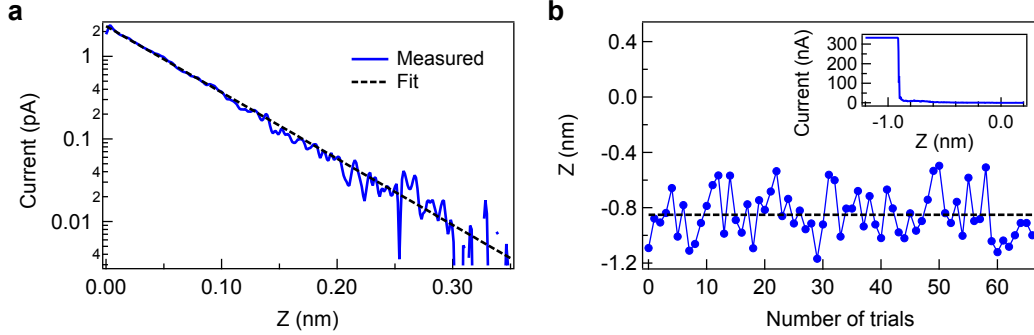

Figure S2 | a, Measured I-Z curve. The data were fitted using $I = exp(-1.025\sqrt{(\varphi_0 - eV/2)Z})$ with the effective work function of $\varphi_0 = 3.8 \pm 0.1$ eV. **b**, The gap width measured by driving the tip into the sample (HOPG). The inset shows a typical I-Z curve. The rapid increase in current at $Z{\sim}0.85$ nm indicates the point of contact. A gap width of 0.85 ± 0.17 nm was determined. Both sets of data were taken from ref. 3.

	Tip 1	Tip 3	Tip 5
R	350 Ω	300 Ω	220 Ω
L	0.100 nH	0.126 nH	0.120 nH
C	0.620 fF	0.434 fF	0.448 fF

Table S1 | Simulation parameters for different nanotips.

III. Electromagnetic simulation for THz near fields at a single tunnel junction

A three-dimensional (3D) finite element calculation was performed using a commercially available software (CST MW STUDIO) to simulate the THz near-field waveform in a tunnel junction. The effect of macroscopic nanotip geometry was investigated by using a Lorentzian function (diameter: 0.3 mm, height: 0.1–0.4 mm) to model the nanotip shape. A grid size of 2.5 µm × 2.5 µm × 2.5 µm and a gap width of 10 µm were used. The p-polarized THz radiation was incident from a source plane with a uniform field distribution and an incident angle of 75° (see Fig. 5a in the main text). The Lorentzian-shaped tip and a sample were modeled as perfect electric conductors. The time evolution of the THz electric field was calculated at the midpoint between the nanotip and the sample. To determine whether the macroscopic or nanoscopic geometrical feature of nanotips is significant to the shape of the THz near-field waveform, we also simulated the THz near field for the tip-sample configuration with nanoscale geometry. A gap width of 1.0 nm and the smallest grid size of 0.5 nm × 0.5 nm× 0.5 nm between the nanotip and the sample were used in the calculation. Although the gap width and the grid size of the nanoscale simulations differed by four orders of magnitude from those of the macroscale simulations, the THz near-field waveforms were almost identical (see Fig. S3). This result indicates that the waveform of the THz near field is affected by the wavelength-scale feature of nanotips, rather than the nanoscale geometrical configuration. We also note that the difference of the gap width only affects the field enhancement of the near field. In the case of the 1 nm gap, the enhancement factor of the peak THz electric field reaches 71,000, which is in good
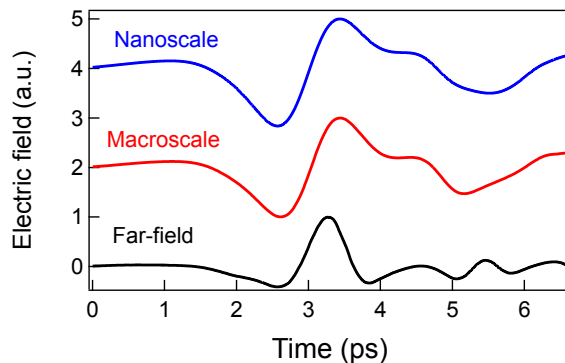

Figure S3 | Comparison of macroscale and nanoscale simulations (tip height in each case: 0.3 mm) performed with a gap width of 1.0 nm and 10 µm, respectively.

agreement with the experimental results as shown in Fig. 4b. On the other hand, in the case of the 10 μm gap, the field enhancement factor is significantly reduced to 8.6.

References

(1) Hirori, H.; Doi, a.; Blanchard, F.; Tanaka, K. *Appl. Phys. Lett.* **2011**, *98*, 091106.

(2) Kawada, Y.; Yasuda, T.; Takahashi, H. *Opt. Lett.* **2016**, *41*, 986.

(3) Reid, M.; Fedosejevs, R. *Appl. Opt.* **2005**, *44*, 149–153.

(4) Yoshioka, K.; Katayama, I.; Minami, Y.; Kitajima, M.; Yoshida, S.; Shigekawa, H.; Takeda, J. *Nat. Photonics* **2016**, *10*, 762–765.

(5) Wang, K.; Mittleman, D. M.; van der Valk, N. C. J.; Planken, P. C. M. *Appl. Phys. Lett.* **2004**, *85*, 2715.

(6) Chen, H.-T.; Kraatz, S.; Cho, G. C.; Kersting, R. *Phys. Rev. Lett.* **2004**, *93*, 267401.

(7) Wimmer, L.; Herink, G.; Solli, D. R.; Yalunin, S. V.; Echternkamp, K. E.; Ropers, C. *Nat. Phys.* **2014**, *10*, 432–436.